Mon. Not. R. Astron. Soc. **000**, 1–11 (2009) Printed 23 February 2009 (MN LATEX style file v2.2)

Optical spectroscopy and Doppler tomography of Cygnus X-2

P. Elebert,[1⋆] P. J. Callanan,[1] M. A. P. Torres[2] and M. R. Garcia[2]
[1] *Department of Physics, University College Cork, Cork, Ireland*
[2] *Harvard–Smithsonian Center for Astrophysics, 60, Garden St., Cambridge, MA 02138, U.S.A.*

23 February 2009

ABSTRACT

We present phase resolved optical spectroscopy and Doppler tomography of V1341 Cygni, the optical counterpart to the neutron star low mass X-ray binary Cygnus X-2. We derive a radial velocity curve for the secondary star, finding a projected radial velocity semi-amplitude of $K_2 = 79 \pm 3$ km s^{-1}, leading to a mass function of 0.51 ± 0.06 M$_\odot$, $\sim$30% lower than the previous estimate. We tentatively attribute the lower value of K_2 (compared to that obtained by other authors) to variations in the X-ray irradiation of the secondary star at different epochs of observations. The limited phase coverage and/or longer timebase of previous observations may also contribute to the difference in K_2. Our value for the mass function implies a primary mass of 1.5 ± 0.3 M$_\odot$, somewhat lower than previous dynamical estimates, but consistent with the value found by analysis of type-I X-ray bursts from this system. Our Doppler tomography of the broad He II λ4686 line reveals that most of the emission from this line is produced on the irradiated face of the donor star, with little emission from the accretion disc. In contrast, the Doppler tomogram of the N III λ4640.64 Bowen blend line shows bright emission from near the gas stream/accretion disc impact region, with fainter emission from the gas stream and secondary star. This is the first LMXB for which the Bowen blend is dominated by emission from the gas stream/accretion disc impact region, without comparable emission from the secondary star. This has implications for the interpretation of Bowen blend Doppler tomograms of other LMXBs for which the ephemeris may not be accurately known.

Key words: accretion, accretion discs – stars: individual: Cygnus X-2, V1341 Cygni – stars: neutron – X-rays: binaries

1 INTRODUCTION

Characterising the mass spectrum of neutron stars (NS) is critical to the understanding of the equation of state (EoS) which describes degenerate nuclear matter (Lattimer & Prakash 2004, 2007). Low mass X-ray binaries (LMXBs) with NS primaries offer a promising means for increasing the number of such mass estimates, and better constraining the NS EoS. For example, van den Heuvel & Bitzaraki (1995) have shown that some neutron stars could accrete up to 0.7 M$_\odot$ over the course of the binary lifetimes. The detection of such massive neutron stars would significantly reduce the range of currently allowable NS equations of state.

LMXBs themselves are sub-divided into transient and persistent systems. Persistent systems are those where the primary is continuously accreting at a significant fraction of the Eddington limit, whereas in transient systems, occasional outbursts are separated by long periods of quiescence, generally explained by the disc instability model (Dubus, Hameury & Lasota 2001).

In quiescent transient systems, the mass of the compact object can be constrained by dynamical studies if the secondary is bright enough. Spectroscopic observations allow both the orbital period and the velocity of the secondary (projected onto the line of sight) to be determined, and these quantities are all that are required to calculate the mass function ($f(M)$), a lower limit to the mass of the primary star. If the optical counterpart is sufficiently bright to allow higher resolution spectroscopy to be performed, the mass ratio can be estimated by measuring the rotational broadening of the absorption lines originating in the secondary star (e.g. Marsh, Robinson & Wood 1994). Finally, fitting of light curves can place constraints on the system's inclination, providing the final piece of information required to constrain the primary mass.

⋆ E-mail: p.elebert@ucc.ie

However, in LMXBs where the optical light is dominated by the accretion disc, other techniques are required to find the system parameters. Specifically, Steeghs & Casares (2002) found that in the case of Scorpius X-1, the Bowen blend emission (a blend of N III and C III emission lines near λ4640) can be used to trace the motion of the secondary star. Doppler tomography of Bowen blend emission lines revealed a bright spot of emission, attributed to Bowen emission from the irradiated surface of the secondary star. This technique has since been used to determine the secondary velocity in a number of other systems (Casares et al. 2004; Cornelisse et al. 2008, and references therein), although we note that no independent verification of K_2 has been obtained for any of these systems to date.

Cyg X-2 is a persistent NS LMXB, discovered in 1965 (Bowyer et al. 1965), and is the second X-ray binary for which an optical counterpart (V1341 Cygni) was found (Giacconi et al. 1967). Orosz & Kuulkers (1999) find that Cyg X-2 is located at a distance of $\sim$7 kpc and the high X-ray flux implies that it is accreting at close to the Eddington limit. It is one of the few persistent systems where the secondary is visible, contributing 70% of the optical flux (Orosz & Kuulkers 1999). Although the spectral type is A9 III (Casares, Charles & Kuulkers 1998), the mass of the secondary (M_2) is $\sim$0.6 $M_\odot$ (see Podsiadlowski & Rappaport 2000, for more details). From the radial velocity (RV) curve based on absorption line spectra from the stellar photosphere, Casares et al. (1998) established that $P_{\rm orb} = 9.8444 \pm 0.0003$ d and $K_2 = 88.0 \pm 1.4$ km s^{-1}, yielding a value for the mass function of the NS in this system of $f(M) = 0.69 \pm 0.03$ $M_\odot$. They also measured the systemic velocity (γ) to be -209.6 ± 0.8 km s^{-1}. Their estimate for the rotational broadening of the secondary star of 34.2 ± 2.5 km s^{-1} constrains the mass ratio, q, to be 0.34 ± 0.04. Setting the lower limit of M_2 in line with the predictions of King et al. (1997) allowed Casares et al. (1998) to constrain the primary mass (M_1) to be greater than 1.88 $M_\odot$, and the orbital inclination (i) to be less than 61°, with 95% confidence. The existence of such a massive NS suggests that a stiffer EoS describes degenerate nuclear matter.

Subsequently, by fitting U-, V- and B-band light curves, Orosz & Kuulkers (1999) found a value for the inclination of $62^\circ.5 \pm 4^\circ$, which combined with the parameters found by Casares et al. (1998) gave a value for the primary mass of 1.78 ± 0.23 $M_\odot$. This latter mass estimate is consistent with the canonical NS mass of 1.4 $M_\odot$ at the 2σ level. Orosz & Kuulkers (1999) also found that X-ray heating of the secondary star contributed very little to the overall light curves, possibly because of the large orbital separation, or because a flared accretion disc is shielding the secondary from the X-rays.

In contrast, analysis of X-ray bursts from Cyg X-2 allowed Titarchuk & Shaposhnikov (2002) to constrain the primary mass to be 1.44 ± 0.06 $M_\odot$, lower than that obtained by previous dynamical studies, and equal to the canonical NS mass of 1.4 $M_\odot$, within the uncertainties.

Here, we present results based on spectroscopic observations of Cyg X-2 taken in 2006 September/October. Our primary motivation for this work was to perform Doppler tomography for this long period system, to study the accretion flow, and especially to make the first comparison between the radial velocity of the secondary as inferred from the Bowen blend technique and absorption line measurements (i.e. Casares et al. 1998). Confirmation of this technique for a system where an independent measure of the radial velocity is available gives further support for using Bowen blend to measure K_2 in situations where the secondary star is not directly observable. In light of the NS mass estimates discussed above, we also used our data to perform a new radial velocity analysis of this system to confirm the suggested massive nature of the NS star primary.

2 DATA

Our data consist of optical spectra, acquired with the FAST spectrograph (Fabricant et al. 1998), at the Cassegrain focus of the 1.5-m Tillinghast telescope at the Fred L. Whipple Observatory, Mt. Hopkins, Arizona. The FAST3 University of Arizona STA520A (SN4377) CCD was used, with 2720×161 15 μm pixels in the binned images. The spectra were taken using the 600 lines mm^{-1} grating, with a 2 arcsec slit, giving a spectral coverage of $\sim$2000 Å. The spectra were obtained on 16 nights in 2006 September and October, covering four orbits. One spectrum was obtained each night, along with HeNeAr arc lamp exposures, bias, flat and dark frames, and one spectrophotometric standard exposure (BD+28°4211). For 14 of the nights, only one arc spectrum was available for the wavelength calibration of each Cyg X-2 spectrum. For the other two nights, the Cyg X-2 exposures were bracketed by arc spectra.

The frames were firstly processed using the IRAF[1] CCDPROC routines to remove instrumental effects. The spectra were then optimally extracted using tasks in the IRAF KPNOSLIT package. Wavelength solutions were found by fitting a 3rd order cubic spline to $\sim$60 – 70 lines in each arc spectrum, giving an RMS error of <0.04 Å, and these solutions were then applied to the target frames. The resulting dispersion was $\sim$0.74 Å pixel^{-1}, with a resolution (measured from arc lines) of $\sim$2.3 Å. For comparison, the observations of Casares et al. (1998) had a resolution of $\sim$0.5 – 0.8 A. Table 1 gives details of our observations. In order to verify the wavelength calibration, the sky lines were examined. Only five sky lines were isolated and strong enough to be useful i.e. with a FWHM similar to the spectral resolution.

For nights where only a single arc spectrum was available, we found that there were significant discrepancies between the measured wavelengths of these sky lines and their rest wavelengths, as much as 0.5 Å. For those nights where the target observations were bracketed by arcs, the interpolated wavelength solution resulted in sky lines at their expected wavelengths.

To correct for these offsets, we used the RVSAO package in IRAF (Kurtz & Mink 1998) to cross-correlate the sky spectra against the sky spectrum from October 16 (which was calibrated using two arc spectra) and applied the measured wavelength shifts to the target spectra. For the two nights where we had two arc spectra, we found that this

[1] IRAF is distributed by the National Optical Astronomy Observatories, which are operated by the Association of Universities for Research in Astronomy, Inc., under cooperative agreement with the National Science Foundation.

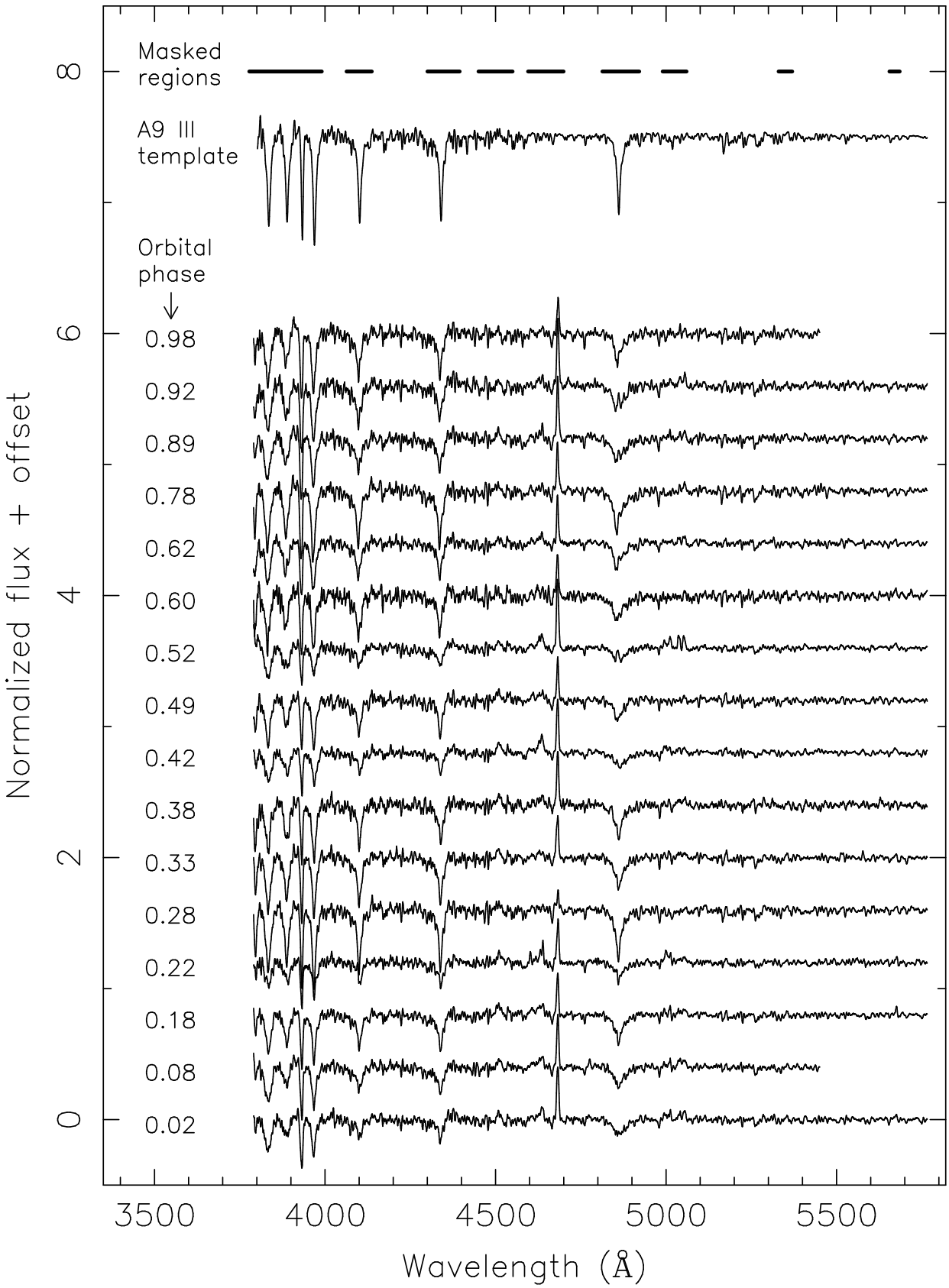

Figure 1. 16 normalized spectra from 2006 September and October, with a vertical offset of 0.4 units. The A9 III template spectrum is also shown. The wavelength regions masked from the cross-correlation are also marked. The spectra have been boxcar smoothed.

Table 1. Observations of Cyg X-2 from 2006 September and October.

Date (UT)	Exp. time (s)	Coverage (Å)	Dispersion (Å)	Orbital phase [b]
Sep 17 [a]	1200	3456 – 5453	0.743	0.98
Sep 18 [a]	1200	3455 – 5453	0.743	0.08
Sep 19	1200	3773 – 5773	0.744	0.18
Sep 20	1200	3780 – 5779	0.744	0.28
Sep 21	869	3779 – 5780	0.744	0.38
Sep 22	1200	3773 – 5773	0.744	0.49
Sep 25	1200	3770 – 5770	0.744	0.78
Sep 26	1178	3774 – 5774	0.744	0.89
Oct 03	1200	3775 – 5775	0.744	0.60
Oct 16	1200	3787 – 5786	0.744	0.92
Oct 17	1200	3786 – 5785	0.744	0.02
Oct 19	1200	3785 – 5784	0.744	0.22
Oct 20	1200	3788 – 5788	0.744	0.33
Oct 21	1200	3768 – 5768	0.744	0.42
Oct 22	1200	3780 – 5780	0.744	0.52
Oct 23	1200	3784 – 5784	0.744	0.62

[a] Data on September 17 and 18 were taken with a slightly different central wavelength to the other nights.
[b] Based on the T_0 found by Casares et al. (1998) and $P_{\rm orb}$ = 9.84456 d.

technique produced a wavelength scale very similar (maximum difference of ∼0.02 Å) to that produced using the two arc spectra.

After applying the sky line correction, the Cyg X-2 spectra were imported into the MOLLY spectral analysis package, where the spectra were shifted to the heliocentric frame, outlying flux values were cleaned and the spectra were rebinned onto a common velocity scale of 50 km s^{-1} pixel^{-1}. We found that the 1σ errors produced by IRAF were significantly lower than the RMS of continuum regions, and that this was different for each of the spectra. Therefore, we increased the errors in each of the spectra to more closely match the RMS. The spectra were rectified by fitting the continuum with a spline function (after masking the major emission and absorption features), dividing by this fit and subtracting unity. Fig. 1 shows these spectra, each with a vertical offset of 0.4 units.

We subsequently obtained spectra of 4 template stars in 2008 September, spanning the range A5 to F1 III (see Casares et al. 1998). The A9 III template (HR2489) is the same as that used by Casares et al. (1998). These frames were processed in an identical manner to the Cyg X-2 frames. However, arc spectra were taken at regular intervals, so the sky line correction procedure as employed for the Cyg X-2 spectra was not required. Inspection of the O III λ5577.34 sky line showed that it was located at the correct wavelength in each calibrated frame. Details of the template observations are given in Table 2. The normalized spectrum for the A9 III template HR2489 is also shown in Fig. 1.

The spectra for each template were averaged and imported into MOLLY, where each spectrum was shifted to the heliocentric reference frame, and the continua removed as for the Cyg X-2 spectra.

Table 2. Observations of template stars from 2008 September.

Date (UT)	Template star	Spectral type	No. obs.	Total exposure time (s)
Sep 24	HD218260	A5 III	3	180
Sep 24	HD220999	A7 III	4	60
Sep 24	HD240431	F1 III	3	270
Sep 25	HR2489	A9 III	9	165

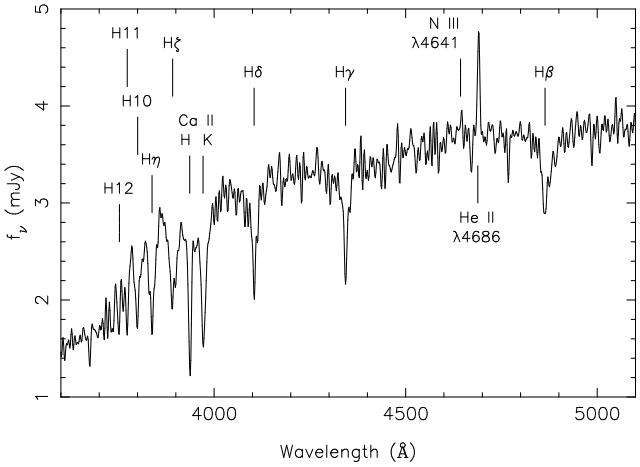

Figure 2. Flux calibrated spectrum from 2006 September 17 UT. The spectrum has been shifted to the rest frame of the system, and the major spectral features have been marked.

3 RESULTS

3.1 Flux calibrated spectrum

For spectra where observing conditions were photometric, flux calibration was performed against the standard star BD+28°4211. Fig. 2 shows the flux calibrated spectrum from 2006 September 17 from which we extracted a B-band magnitude of 15.2 mag. This is consistent with the mean value over two decades reported by Orosz & Kuulkers (1999) of 15.2 ± 0.2 mag (where the error reflects the RMS error of all the values). Also, visual comparison of our spectrum with those of van Paradijs et al. (1990) and O'Brien et al. (2004) shows that the spectrum is very similar at these epochs.

The equivalent widths (EW) and full-width half-maxima (FWHM) of the absorption and emission lines in the average of all 16 spectra are shown in Table 3.

The strongest feature in the Bowen blend in the average spectrum is at a wavelength of λ4637.4. Assuming a systemic velocity of −210 km s^{-1} (Casares et al. 1998), we identify this emission as from the N III λ4640.64 line. This is frequently observed to be the strongest line in the Bowen blend (Casares et al. 2004). There does not appear to be any significant emission from the other lines normally present in the Bowen blend. However, because of the resolution of our spectra, emission from these lines may be present but blended with that from the N III λ4640.64 line.

Table 3. EW and FWHM of the emission and absorption lines in the averaged Cyg X-2 spectrum.

Line	EW (Å)	FWHM (Å)
He II λ4686	-2.9 ± 0.1	6.4 ± 0.2
Bowen blend	-0.8 ± 0.1	.....
Hβ	5.2 ± 0.1	33 ± 2
Hγ	4.4 ± 0.1	18 ± 2
Hδ	4.5 ± 0.1	18 ± 2
Hζ	3.6 ± 0.1	18 ± 2
Hη	6.1 ± 0.1	19 ± 2

3.2 Radial velocity study

As the primary motivation for this work was to produce Doppler tomograms, we initially did not observe any radial velocity templates. However, by using the individual spectra as templates, we were able to derive a radial velocity curve, which suggested that K_2 was significantly lower than the value obtained by Casares et al. (1998). In order to confirm this lower value of K_2, we later obtained spectra of 4 template stars, including the A9 III template used by Casares et al. (1998). and we cross-correlated the Cyg X-2 spectra against these templates to obtain radial velocities.

For the cross-correlation, the broad Balmer absorption features, Ca II H and K lines, and emission lines were masked (see Fig. 1). The trailed spectrogram in Fig. 3 shows a subset of the data used in the cross-correlation ($\lambda\lambda$4900 – 5000). The S-waves due to the narrow absorption lines from the secondary are clearly visible. The cross-correlations also took into account the uncertainties in the wavelength solution of each of the spectra, as well as the slight differences in the cross-correlation value when different interpolations/binnings were used. This was accomplished by running 10000 cross-correlations for each spectrum-template pair. For each cross-correlation, the wavelength scale of the spectrum and template were shifted independently by choosing a shift value from a Gaussian distribution with a mean of 0 and standard deviation equal to the estimated uncertainty in the wavelength solution due to the arc line fitting and the sky line correction.

We fit the 4 RV curves (derived from cross-correlation against the 4 templates) using both circular and elliptical orbit models. Using the Lucy & Sweeney (1971) test, we found that an elliptical orbit was not a significant improvement over a circular orbit for any of these 4 RV curves: the eccentricity (e) in each case was $\sim 0.06 \pm 0.04$. With a circular orbit and 3 free parameters (K_2, γ and $P_{\rm orb}$, with T_0 set to the value found by Casares et al. (1998)), a sine fit to each of these 4 RV curves gave almost identical results (to better than 1σ). Using the same A9 III template as used by Casares et al. (1998), we found $K_2 = 79 \pm 3$ km s^{-1}, $P_{\rm orb} = 9.84456 \pm 0.00012$ d and $\gamma = -212 \pm 2$ km s^{-1}, where the radial velocity of the template of 7.7 ± 0.1 km s^{-1} (Gontcharov 2006) has been included. This is in contrast to the values found by Casares et al. (1998). For comparison, Casares et al. (1998) found values of $K_2 = 88.0 \pm 1.4$ km s^{-1} $P_{\rm orb} = 9.8444 \pm 0.0003$ d and $\gamma = -209.6 \pm 0.8$ km s^{-1}. The uncertainties in our measurements, here and in the remainder of the paper, are 1σ and were determined using Monte Carlo simulations assuming Gaussian statistics. The values we obtained for $P_{\rm orb}$ and γ are consistent at approximately the 1σ level with the values determined by Casares et al. (1998). However, the K_2 values differ at the 99.7% level. The RV curve obtained from cross-correlation against the A9 III template star and best-fitting circular orbit are shown in Fig. 4. The reduced χ^2 (χ^2_ν) for this fit is 1.2 for 13 degrees of freedom. For comparison, the RV curve generated using the parameters of Casares et al. (1998) is also shown.

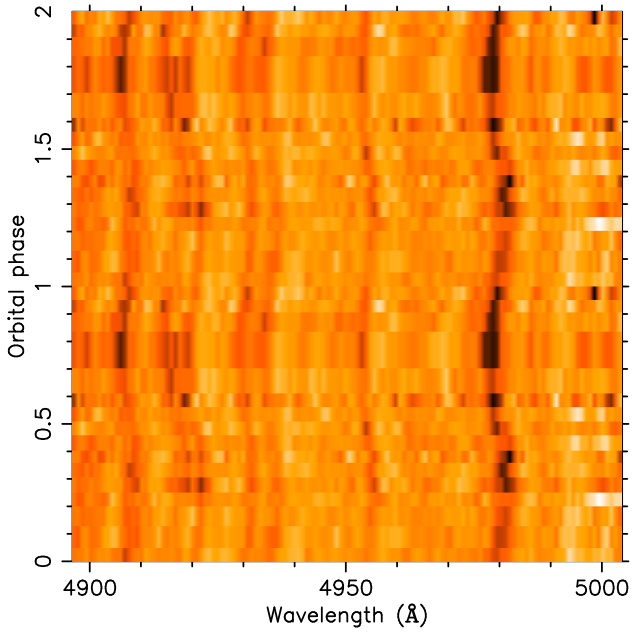

Figure 3. Trailed spectrogram for the data between $\lambda\lambda$4900 and 5000, showing some of the narrow absorption lines from the secondary.

3.3 System parameters

Using the mass function equation and the values for K_2 and $P_{\rm orb}$ gives a value for the mass function of $f(M) = 0.51 \pm 0.06$ M$_\odot$. Because of the higher resolution spectroscopy of Casares et al. (1998), we use their value for the rotational broadening of the secondary star, $v \sin i = 34.2 \pm 2.5$ km s^{-1}. Combined with our lower value of K_2, we find a mass ratio of $q = 0.42 \pm 0.06$. Along with our value for $f(M)$, we calculate $M_1 \sin^3 i = 1.03 \pm 0.15$ M$_\odot$.

X-ray eclipses have not been observed from this system, and this allows us to set a firm upper limit to the inclination. Re-arranging the equation of Paczyński (1971), we get:

$$\frac{r_2}{a} = 0.462 \left(\frac{q}{q+1} \right)^{\frac{1}{3}}$$

where a is the binary separation and r_2 is the radius of the secondary star.

In order for the secondary not to eclipse the primary, the upper limit on the inclination is $90^\circ - \tan^{-1} \frac{r_2}{a}$ which is $72^\circ.7 \pm 0^\circ.6$. This angle is relatively insensitive to changes in q. Using this limit, we place a lower limit on the primary mass of $M_1 > 1.18 \pm 0.17$ M$_\odot$.

Orosz & Kuulkers (1999) find a lower limit to the orbital inclination by fitting the ellipsoidal modulation in their

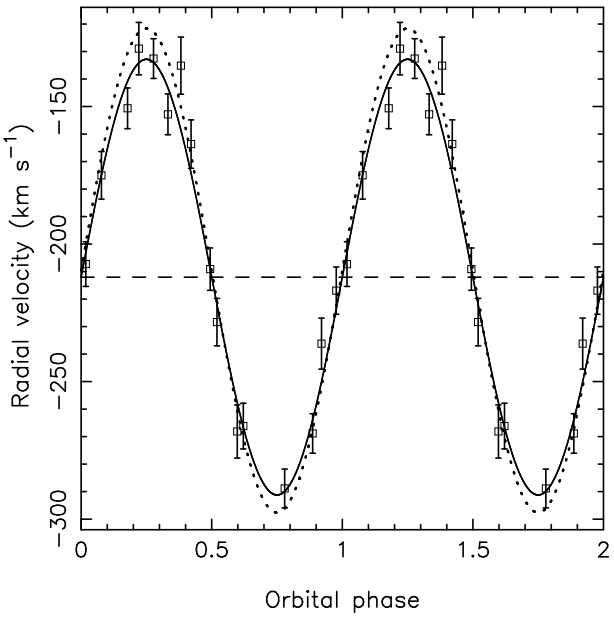

Figure 4. Radial velocity curve derived using the A9 III star HR2489 as a template. The best-fitting circular orbit is also plotted, and the γ value of -212 km s^{-1} is marked with a dashed line. The curve of Casares et al. (1998) is plotted with a dotted line. Two phases are shown for clarity.

V-band light curve, assuming no contribution from the disc or from an irradiated secondary – both of these would dilute the observed modulation, and so the inclination found when these effects are not included is a lower limit. Taking the published V-band data of Orosz & Kuulkers (1999), we used the ELC (Eclipsing Light Curve: Orosz & Hauschildt 2000) code to fit the modulation, using the parameters described in Orosz & Kuulkers (1999), and reproduced their value for the inclination lower limit[2] of $\sim$49° (48°.7 $\pm$ 2°.1). We then adjusted the ELC parameters for $P_{\rm orb}$, $f(M)$ and q based on our spectroscopic results, and found the best fit was for $i = 49°.8 \pm 2°.0$. This sets an upper primary mass limit of 2.3 ± 0.4 M$_\odot$.

We then re-fit both the B- and V-band light curves of Orosz & Kuulkers (1999) with ELC, with X-ray irradiation and the contribution from the accretion disc included. We adjusted the parameters for $P_{\rm orb}$, $f(M)$ and q as before, and by optimizing the inclination and disc temperature parameters[3] found a best-fitting inclination of $i = 63 \pm 3°$, almost identical to the value found by Orosz & Kuulkers (1999) of $i = 62.5 \pm 4°$. The uncertainty was computed in a similar manner to Orosz & Kuulkers (1999). Combining this inclination estimate with our value of $M_1 \sin^3 i = 1.03 \pm 0.15$ M$_\odot$, we obtained a primary mass of $M_1 = 1.5 \pm 0.3$ M$_\odot$, and a secondary mass of $M_2 = 0.63 \pm 0.16$ M$_\odot$.

[2] Note that Orosz & Kuulkers (1999) found lower limits of 42° and 49° for the B and V-band light curves, respectively, and so adopted 49° as a lower limit.

[3] The equation in ELC which describes the disc temperature as a function of radius is different to that used by Orosz & Kuulkers (1999), so we therefore firstly adjusted the temperature parameters to give the same disc temperature profile as used by Orosz & Kuulkers (1999) before optimizing these parameters.

3.4 Doppler tomography

Doppler tomography is an inversion technique where a velocity space image of the accretion disc, gas stream and secondary star is generated using phase resolved spectroscopy (Marsh & Horne 1988; Marsh 2001); the observed spectra are projections of the system at different orbital phases. A Doppler tomogram is a two dimensional image in velocity space ($V_{\rm x}$,$V_{\rm y}$), with intensity representing strength of emission at a particular velocity. The Doppler tomograms presented here were constructed using the maximum entropy method (MEM), as implemented in the DOPPLER package. Synthetic line profiles, created from an initial tomogram of constant pixel values, were fitted to the observed line profiles, by varying the pixel values. This process was continued until the χ^2_ν of the fit approached a target value. As a large number of tomograms can satisfy a particular target χ^2_ν, the tomogram with the maximum entropy (i.e. the smoothest image) was chosen. The entropy was defined relative to a Gaussian blurred default image. We obtained similar tomograms using the filtered back-projection technique implemented in MOLLY, where the tomogram is created by smearing the filtered line profiles across the image in directions determined by the orbital phases of the profiles.

3.4.1 He II *λ4686 emission line*

Fig. 6 shows the Doppler tomogram for the He II λ4686 emission line. This emission line is often seen in X-ray binaries, and is formed by reprocessing of soft X-rays from the central source. The Roche lobe of the secondary is plotted, for $K_2 = 79$ km s^{-1} and $q = 0.42$ (see Section 3.2), as is the centre of the mass of the system, marked by a $*$. The lower curve is the gas stream velocity from the inner Lagrangian point, and the upper curve is the velocity of the accretion disc along the gas stream. The main feature to note is that most of the emission comes from near the secondary star, although there is also a much broader region of faint emission, due to the accretion disc. with a distribution typical of that seen in accretion discs in other LMXBs.

Fig. 7 also shows the Doppler tomogram for the He II λ4686 emission line, focussing on the emission from near the secondary star – the colour bar has been scaled to show only the peak emission. This tomogram shows that the peak of the emission arises on the inner face of the secondary star. The centroid of this emission is at a velocity of $K_{\rm y} = 64 \pm 15$ km s^{-1}.

3.4.2 N III *λ4640.64 emission line*

Fig. 8 shows the trailed spectrogram for the region near λ4640. Because the systemic velocity has not been shifted out, the N III λ4640.64 line appears near λ4638. Although the S/N is low, it does appear that the S-wave for this line leads some of the other S-waves present, (which are due to the motion of the secondary star).

Fig. 9 shows the corresponding Doppler tomogram, again with the Roche lobe and gas stream overplotted. The strongest emission is from the location of the gas stream/accretion disc impact region, with broad, fainter emission from the gas stream and near the secondary. This

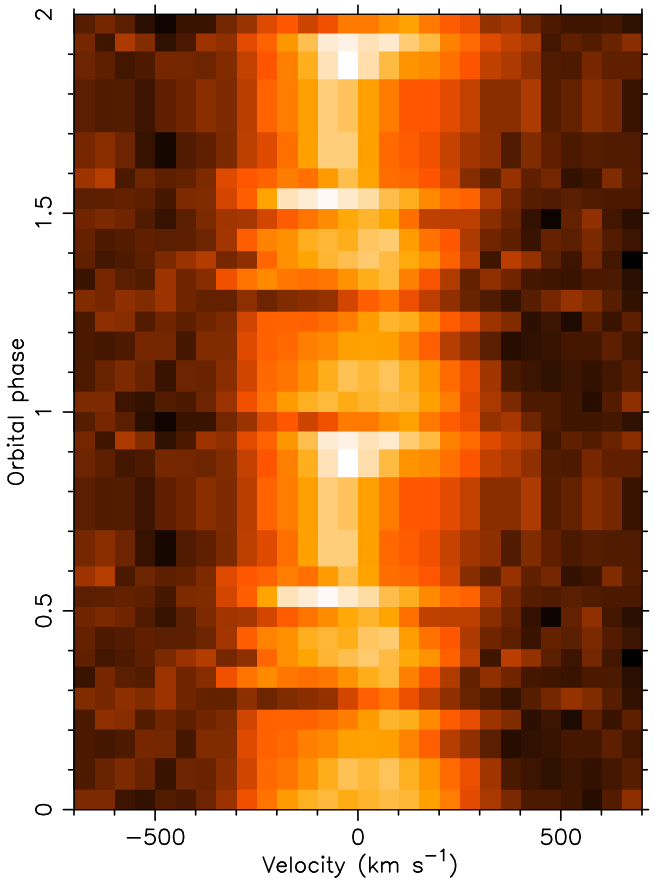

Figure 5. Trailed spectrogram of the data used to construct the He II Doppler tomograms.

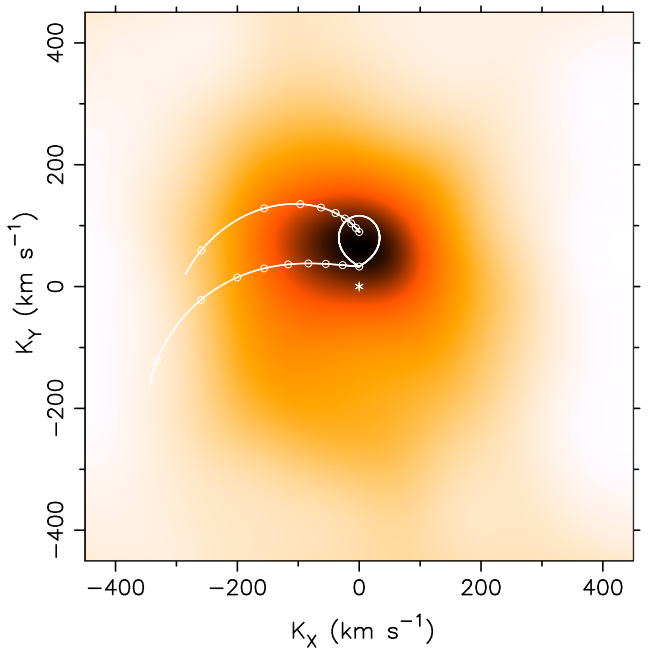

Figure 6. Doppler tomogram of the He II λ4686 emission line. The gas stream and Roche lobe of the secondary are overplotted for $K_2 = 79$ km s^{-1} and $q = 0.42$.

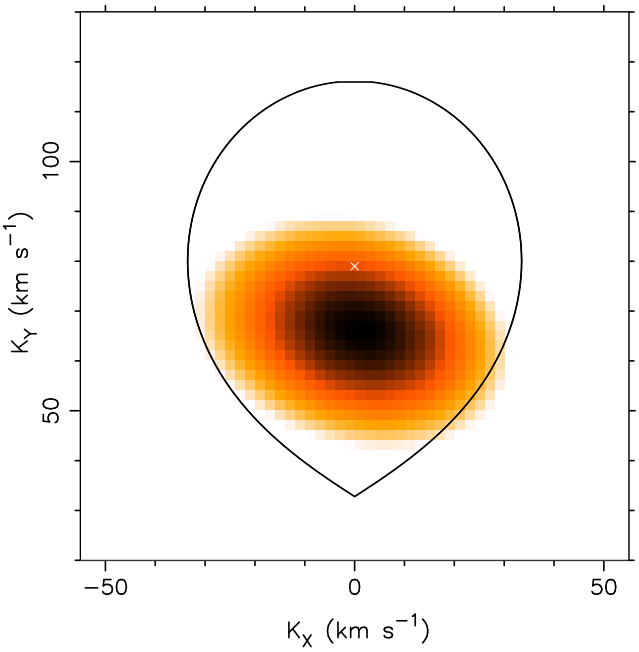

Figure 7. Doppler tomogram of the He II λ4686 emission line, focussed on the region of the secondary star. The Roche lobe of the secondary is overplotted for $K_2 = 79$ km s^{-1} and $q = 0.42$. The position of the secondary is marked with an error bar.

is consistent with the situation we see in the trailed spectrogram (Fig. 8). The overplotted S-wave has a phase offset of 45°, similar to what we see in the Doppler tomogram.

4 DISCUSSION

4.1 Projected velocity of the secondary star

Our value for K_2 differs from the most recent observations of this system by Casares et al. (1998); Table 4 summarises the values for γ and K_2 found by various authors. Because the work of Casares et al. (1998) and our work show that the orbit is most likely circular, we also re-fit the data published by Cowley, Crampton & Hutchings (1979) and Crampton & Cowley (1980) assuming a circular orbit.

In our work, and in the work of Casares et al. (1998) the non-metal lines and the Ca II lines were masked out during cross-correlation (see Fig. 1). Therefore all values of K_2 and γ in Table 4 are essentially based on the velocities of the metal absorption lines.

We now examine possible reasons for our lower value of K_2 compared to that of Casares et al. (1998). Firstly, it is possible that there are systematic errors in our wavelength solution, given that for most of our spectra only a single arc lamp exposure was available, and a correction based on the sky spectra was required. However, our RV curves appear to be quite sinusoidal, which would be unlikely if each spectrum had random errors in the wavelength calibration – indeed, the RV curve from the uncorrected spectra deviates considerably from a sinusoid. Also as we mention in Section 2, for the cases where we had two arc spectra, the maximum difference between the wavelength solutions using the two arc spectra, and using the sky line correction technique is

Table 4. K_2 and γ found by different authors.

Source	Start of observations	End of observations	Time base	Method used	K_2 (km s^{-1})	γ (km s^{-1})
a	1975 June 03	1978 August 09	3.2 yr	Metal lines	87 ± 3	-222 ± 2
b	1975 June 03	1978 August 09	3.2 yr	Metal lines	89 ± 5	-222 ± 4
c	1979 July 02	1979 September 17	77 d	Metal lines	80 ± 6	-203 ± 3
d	1979 July 02	1979 September 17	77 d	Metal lines	75 ± 4	-202 ± 2
e	1993 December 16	1997 August 07	3.6 yr	Cross correlation	88.0 ± 1.6	-209.6 ± 0.8
f	2006 September 17	2006 October 23	35 d	Cross correlation	79 ± 3	-212 ± 2

(a) KPNO data of Cowley et al. (1979).
(b) Based on our re-fitting of the KPNO data of Cowley et al. (1979) assuming a circular orbit.
(c) Crampton & Cowley (1980).
(d) Based on our re-fitting of the data of Crampton & Cowley (1980) assuming a circular orbit.
(e) Casares et al. (1998).
(f) This paper.

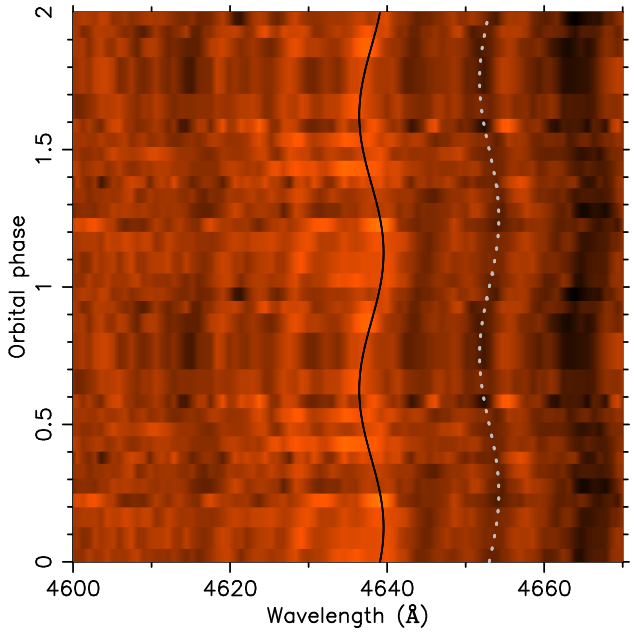

Figure 8. Trailed spectrogram of the data near the N III λ4640.64 emission line. The systemic velocity has not been removed, so the N III λ4640.64 line is near λ4638. The solid line marks the S-wave from N III λ4640.64 emission, while the dotted line marks one of the nearby secondary absorption lines.

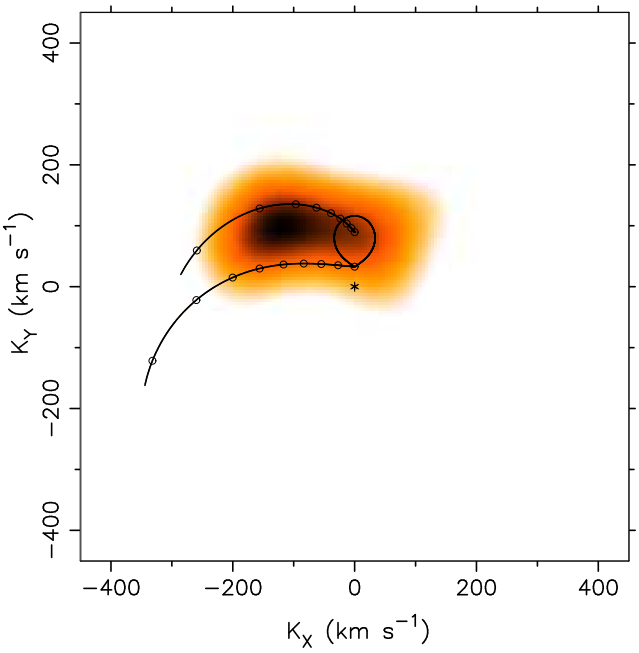

Figure 9. Doppler tomogram of the N III λ4640.64 emission line. The gas stream and Roche lobe of the secondary are overplotted for $K_2 = 79$ km s^{-1} and $q = 0.42$.

$\sim$0.02 Å, or $\sim$1.3 km s^{-1} at λ4686. Our RV curves include the uncertainties in wavelength scales, and also the slight differences in the cross-correlation values that arise when different interpolations are used. Finally, we find a value for γ almost identical to that found by Casares et al. (1998), which would again be improbable if there were any systematic errors in our wavelength scales.

Hence, we believe our measurement of K_2 to be accurate, and so we require an alternative explanation for the difference between this measurement and that of Casares et al. (1998). Because our He II Doppler tomography confirms that the secondary is irradiated by X-rays from the central source, the absorption lines from the irradiated face of the secondary star may be weaker than those from the non-irradiated face. The irradiation of the secondary may be such that the absorption lines are completely quenched on the irradiated hemisphere of the secondary star. In this case, an RV curve based on the velocity of absorption lines from the secondary star will result in a K_2 value which reflects the velocity of the non-irradiated hemisphere. This is larger than the velocity of the centre of mass of the secondary star. If the irradiation of the secondary was variable, such that at some phases the absorption lines on the irradiated face of the secondary were not fully quenched, then one would expect the K_2 value derived from the resulting RV curve to lie somewhere between the true value and the maximum value obtained for complete quenching. See Wade & Horne (1988) for further discussion of this effect. Steeghs & Jonker (2007) argue that differences in K_2 found by different authors for

the LMXB 2S 0921−630 may be due to variable irradiation effects, and we suggest that the same may well apply in the case of Cyg X-2. Clarkson et al. (2003) show that the long term X-ray variability in Cyg X-2 can be explained by a precessing warped accretion disc. The changing orientation of this disc warp will cause the irradiation of the secondary to vary (see also Vrtilek et al. 2003).

To estimate the effects of irradiation for Cyg X-2, we use the approach of Wade & Horne (1988). If the absorption centre of the secondary star is displaced from the centre of mass by an amount $\Delta r = fr_2$, where r_2 is the radius of the secondary star and f is the fractional displacement, then:

$$\Delta K_2 = \frac{\Delta r}{a_2} K_2$$

where a_2 is the separation between the secondary and the binary centre of mass. Based on our new value for q, $a_2 = 0.70a$. Using the formula of Paczyński (1971), the radius of the secondary is $0.31a$. Therefore, $\Delta K_2 = 0.443 f K_2$. In the extreme case, where there is no absorption from the inner hemisphere of the secondary star, $f = 4/(3\pi)$, and $\Delta K_2 = 0.19 K_2 \simeq 15$ km s^{-1}. Therefore, we find that the measured value of K_2 can be as much as $\sim$15 km s^{-1} greater than the true value. This difference is more than enough to explain the different values found by various authors.

In order to investigate the effect of irradiation on the absorption features of the secondary in Cyg X-2, we show in Fig. 10 the EW of the Fe I λ5227.15 absorption line as a function of the EW of He II λ4686 (which we take as indicative of the intensity of the X-rays intercepted by the secondary star). This shows that, for this line at least, the stronger the He II λ4686 emission line (and hence X-ray flux), the weaker the secondary absorption line.

On the other hand, a Doppler tomogram of the Ca I λ4227 absorption line shows that the peak occurs at a value consistent with that found in our RV analysis. However, the EW of this line does not show any trend when plotted against the EW of the He II λ4686 emission line. This may suggest that this particular line is less susceptible to the effects of irradiation than other lines (e.g. the Fe I λ5227.15 line), and that the radial velocity determined from this line more accurately reflects the motion of the centre of mass of the secondary star. Because irradiation of the secondary star causes the measured K_2 to be greater than the true value, our measurement of a lower value may be closer to the true value than the estimates of Cowley et al. (1979) and Casares et al. (1998).

We also note from Table 4 that observations obtained over a shorter time base (Crampton & Cowley 1980, and this work) appear to suggest systematically lower values of K_2 than those obtained over a longer period (Cowley et al. 1979; Casares et al. 1998). We speculate that observations obtained over a longer timebase, and wider range of disc precession phase (e.g. Clarkson et al. 2003), result in more variable irradiation of the secondary star. It is possible that the changing values of ΔK_2 that result from this may explain the variation in K_2 we observe.

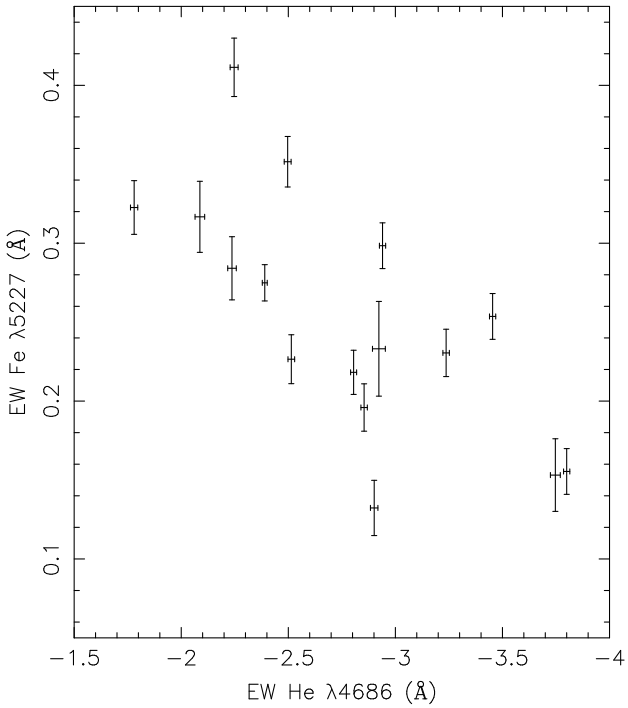

Figure 10. EW of the Fe I λ5227.15 absorption line vs. the EW of the He II λ4686 emission line. Assuming that the EW of the He II λ4686 emission line is correlated with the intensity of the X-rays intercepted by the secondary star, this relationship shows that the EW of the Fe I λ5227.15 absorption line decreases with increasing X-ray flux.

4.2 Primary mass and distance

Our results indicate that the mass of the NS in Cyg X-2 ($M_1 = 1.5 \pm 0.3$ M$_\odot$) is typical of a canonical NS, a downward revision of the previous estimates of a 95% confidence lower limit of 1.88 M$_\odot$ (Casares et al. 1998) and 1.78 ± 0.23 M$_\odot$ (Orosz & Kuulkers 1999). It is interesting to note that the LMXB 2S 0921−630 has also recently had its primary mass estimate reduced, from 3.2 ± 1.2 M$_\odot$ (Shahbaz et al. 2004) to 1.37 ± 0.13 M$_\odot$ (Shahbaz & Watson 2007) and 1.44 ± 0.10 M$_\odot$ (Steeghs & Jonker 2007). Our dynamical mass estimate for the NS in Cyg X-2 is consistent with the mass estimate of Titarchuk & Shaposhnikov (2002) ($M_1 = 1.44 \pm 0.06$ M$_\odot$), based on observations of type-I X-ray bursts from this system.

Calculations by Orosz & Kuulkers (1999) found that there are inconsistencies between the distance based on their optical observations ($d = 7.2 \pm 1.1$ kpc) and the distance estimate of Smale (1998) based on X-ray observations of a type-I radius-expansion burst ($d = 11.6 \pm 0.3$ kpc). To address this, we now re-calculate the distance and observed absolute visual magnitude (M_V) of Cygnus X-2, and compare the latter with the expected value based on our new parameters.

Taking the peak X-ray flux of 1.52×10^{-8} erg cm^{-2} s^{-1} (Smale 1998) to be at the Eddington limit, and with $M_1 = 1.5 \pm 0.3$ M$_\odot$, the Eddington luminosity of the system is $2.0 \pm 0.4 \times 10^{38}$ erg s^{-1} (assuming cosmic composition) and the distance to the source is therefore 10.4 ± 1.0 kpc. With $V = 14.8$ mag, and $A_V = 1.24 \pm 0.22$ mag (McClintock et al. 1984; Orosz & Kuulkers 1999), this gives $M_V = -1.5 \pm 0.3$ mag for the system.

Assuming a secondary star with a surface temperature of $T_2 = 7000 \pm 250$ K (Orosz & Kuulkers 1999),

$M_1 = 1.5 \pm 0.3$ M$_\odot$ and $q = 0.42 \pm 0.06$, the radius of the Roche lobe of the secondary star is 7.6 ± 0.7 R$_\odot$ (Eggleton 1983). Hence, we calculate that the M_V of the secondary should be -0.47 ± 0.25 mag. With a V-band disc fraction ($k_V \equiv f_{disc}/(f_2 + f_{disc})$) of 0.30 ± 0.05 (Orosz & Kuulkers 1999), the absolute magnitude of the system should therefore be -0.86 ± 0.26 mag. This is marginally consistent with the expected value for this system, calculated above assuming a distance of 10.4 ± 1.0 kpc. These estimates would better agree if the secondary temperature was slightly higher. Indeed, we note that the spectral classification of Casares et al. (1998) is A9 $\pm$ 2 subtypes, and an A7 star (with a surface temperature of 7700 ± 300 K) would yield $M_V = -0.88 \pm 0.26$ mag for the secondary and -1.27 ± 0.27 mag for the system as a whole, leading to a distance of 9.4 ± 1.5 kpc. Hence, we conclude that the absolute magnitude calculated from the observed apparent magnitude and the distance based on X-ray measurements is consistent with the expected absolute magnitude based on the spectral type, surface temperature, disc fraction, primary mass and mass ratio.

For many systems, the secondary star dominates the infrared light, and fitting the ellipsoidal modulation in the IR light curves can be used to better constrain the inclination. For Cyg X-2, such a scenario would be particularly desirable, as the modulation in the optical light curves is dominated by variable contamination from the accretion disc. The *2MASS* K-band magnitude of Cyg X-2 is $\sim$13.05 mag. Using $E(B-V) = 0.4$ (McClintock et al. 1984), $A_K/E(B-V) = 0.38$ (Savage & Mathis 1979) and a distance of 10.4 kpc, the dereddended absolute K-band magnitude is $M_K = -2.2 \pm 0.2$ mag. If the secondary is an A7 star, then $V - K \simeq 0.8$ mag. Using the absolute V-band magnitude for the secondary of -0.88 ± 0.26 mag (calculated above), M_K for the secondary should be $\sim -1.7 \pm 0.3$ mag. To achieve the observed M_K for the system of -2.2 ± 0.2 mag would require a K-band disc fraction of $k_K = 0.37^{+0.18}_{-0.25}$. Therefore, it would appear that even in the K-band, the accretion disc contributes a considerable fraction of the light.

4.3 Doppler tomography

Our Doppler tomography shows that the peak of the He II emission originates on the inner hemisphere of the donor star. This is consistent with the results of Vrtilek et al. (2003), who find that the emission lines in their UV spectra also appear to originate in the secondary star. There appears to be little or no emission from the gas stream/accretion disc impact region. Curiously, Orosz & Kuulkers (1999) find that the optical light curves show no evidence for heating of the secondary star, yet our He II Doppler tomograms show that the secondary is certainly intercepting X-rays from the primary. It is unclear how the secondary could be irradiated by the central source, and yet the light curves show no evidence for heating.

The situation is reversed in the N III λ4640.64 tomogram (Fig. 9) , where the majority of the emission arises at the location of the hotspot, between the gas stream trajectory and the velocity of the accretion disc along the gas stream.

Generally, the Bowen blend contains several lines, with the strongest normally being the N III λ4640.64 line. However, in our data, this is the only line which is clearly visible. The location of the emission in the Doppler tomogram shows that significant Bowen blend emission can occur from sources other than the secondary star in LMXBs. This is in contrast to the suggestion by Cornelisse et al. (2008) that the velocity of the Bowen blend emission can be used universally to determine the orbital velocity of the secondary star.

5 CONCLUSIONS

By cross-correlating our spectra against template spectra, we find a value for the projected radial velocity semi-amplitude of the secondary which is significantly lower then that found by Casares et al. (1998). Based on this new value for K_2, we find a larger value for the mass ratio, using the rotational broadening value calculated by Casares et al. (1998). Combined with the inclination estimates by Orosz & Kuulkers (1999), this implies that the mass of the primary in this system is 1.5 ± 0.3 M$_\odot$, less massive than previously determined, although still consistent with the mass estimate of Orosz & Kuulkers (1999) at the 1σ level, and similar to the value found by Titarchuk & Shaposhnikov (2002) based on observations of type-I X-ray bursts.

We have presented Doppler tomograms of Cyg X-2, the first Doppler tomography of such a long period system. Our tomography of the He II λ4686 emission line shows that the majority of the emission is from near the irradiated face of the secondary, with much weaker emission from the accretion disc. Doppler tomography of the N III λ4640 emission line shows that the emission is primarily from the gas stream/accretion disc impact region. The N III tomography demonstrates that care must be taken when interpreting Bowen blend tomograms, so that the hotspot is not confused with the secondary, particularly for systems where the ephemeris is not accurately known.

The measured value of K_2 can vary by up to 15 km s^{-1}, depending on the irradiation of the secondary star by the central X-ray source, and this may explain the differences in K_2 found by different authors. Further investigation of the effects of irradiation of the secondary star – for example, by performing a series of radial velocity studies over a range of disc precession phases – is required to fully understand how large this effect is on the mass estimate of the neutron star in Cyg X-2.

ACKNOWLEDGMENTS

We acknowledge the use of the 1.5-m Tillinghast telescope at Fred L. Whipple Observatory, Mt. Hopkins, Arizona, and we thank observers M. L. Calkins, P. Berlind, T. M. Currie, E. E. Mamajek and W. Peters. We thank S. Tokarz, N. Caldwell and N. Martimbeau for assistance with the sky line correction to the wavelength calibration. This research made use of NASA's Astrophysics Data System, and the SIMBAD database, operated at CDS, Strasbourg, France. This publication makes use of data products from the Two Micron All Sky Survey, which is a joint project of the University

of Massachusetts and the Infrared Processing and Analysis Center/California Institute of Technology, funded by the National Aeronautics and Space Administration and the National Science Foundation. We thank J. A. Orosz for providing us with the ELC code. We acknowledge the use of MOLLY and DOPPLER software packages developed by T. R. Marsh, University of Warwick. We thank the anonymous referee for the helpful suggestions which improved our paper. PE and PJC acknowledge support from Science Foundation Ireland. MRG acknowledges partial support from NASA contract NAS8-03060 to the Chandra X-ray Center.

REFERENCES

Bowyer S., Byram E. T., Chubb T. A., Friedman H., 1965, Annales d'Astrophysique, 28, 791
Casares J., Charles P. A., Kuulkers E., 1998, ApJ, 493, L39
Casares J., Steeghs D., Hynes R. I., Charles P. A., Cornelisse R., O'Brien K., 2004, in Tovmassian G., Sion E., eds, Revista Mexicana de Astronomia y Astrofisica Conference Series Vol. 20, Bowen Fluorescence from Companion Stars in X-ray Binaries. pp 21–22
Clarkson W. I., Charles P. A., Coe M. J., Laycock S., 2003, MNRAS, 343, 1213
Cornelisse R., Casares J., Muñoz-Darias T., Steeghs D., Charles P., Hynes R., O'Brien K., Barnes A., 2008, in American Institute of Physics Conference Series Vol. 1010, An Overview of the Bowen Survey: Detecting Donor Star Signatures in Low Mass X-ray Binaries. pp 148–152
Cowley A. P., Crampton D., Hutchings J. B., 1979, ApJ, 231, 539
Crampton D., Cowley A. P., 1980, PASP, 92, 147
Dubus G., Hameury J.-M., Lasota J.-P., 2001, A&A, 373, 251
Eggleton P. P., 1983, ApJ, 268, 368
Fabricant D., Cheimets P., Caldwell N., Geary J., 1998, PASP, 110, 79
Giacconi R., Gorenstein P., Gursky H., Usher P. D., Waters J. R., Sandage A., Osmer P., Peach J. V., 1967, ApJ, 148, L129
Gontcharov G. A., 2006, Astronomy Letters, 32, 759
King A. R., Frank J., Kolb U., Ritter H., 1997, ApJ, 484, 844
Kurtz M. J., Mink D. J., 1998, PASP, 110, 934
Lattimer J. M., Prakash M., 2004, Science, 304, 536
Lattimer J. M., Prakash M., 2007, Phys. Rep., 442, 109
Lucy L. B., Sweeney M. A., 1971, AJ, 76, 544
Marsh T. R., 2001, in Boffin H. M. J., Steeghs D., Cuypers J., eds, Astrotomography, Indirect Imaging Methods in Observational Astronomy Vol. 573 of Lecture Notes in Physics, Springer Verlag, Berlin, Doppler tomography. pp 1–23
Marsh T. R., Horne K., 1988, MNRAS, 235, 269
Marsh T. R., Robinson E. L., Wood J. H., 1994, MNRAS, 266, 137
McClintock J. E., Remillard R. A., Petro L. D., Hammerschlag-Hensberge G., Proffitt C. R., 1984, ApJ, 283, 794
O'Brien K., Horne K., Gomer R. H., Oke J. B., van der Klis M., 2004, MNRAS, 350, 587
Orosz J. A., Hauschildt P. H., 2000, A&A, 364, 265
Orosz J. A., Kuulkers E., 1999, MNRAS, 305, 132
Paczyński B., 1971, ARA&A, 9, 183
Podsiadlowski P., Rappaport S., 2000, ApJ, 529, 946
Savage B. D., Mathis J. S., 1979, ARA&A, 17, 73
Shahbaz T., Casares J., Watson C. A., Charles P. A., Hynes R. I., Shih S. C., Steeghs D., 2004, ApJ, 616, L123
Shahbaz T., Watson C. A., 2007, A&A, 474, 969
Smale A. P., 1998, ApJ, 498, L141
Steeghs D., Casares J., 2002, ApJ, 568, 273
Steeghs D., Jonker P. G., 2007, ApJ, 669, L85
Titarchuk L., Shaposhnikov N., 2002, ApJ, 570, L25
van den Heuvel E. P. J., Bitzaraki O., 1995, in Alpar M. A., Kiziloglu U., van Paradijs J., eds, The Lives of the Neutron Stars Evolution of Binaries with Neutron Stars. p. 421
van Paradijs J. et al., A. P., 1990, A&A, 235, 156
Vrtilek S. D., Raymond J. C., Boroson B., McCray R., Smale A., Kallman T., Nagase F., 2003, PASP, 115, 1124
Wade R. A., Horne K., 1988, ApJ, 324, 411

This paper has been typeset from a TEX/ LATEX file prepared by the author.